



# Episymbiotic Saccharibacteria TM7x modulates the susceptibility of its host bacteria to phage infection and promotes their coexistence

Qiu Zhong<sup>a,1</sup>, Binyou Liao<sup>b,1</sup> , Jiazen Liu<sup>a,1</sup>, Wei Shen<sup>c</sup>, Jing Wang<sup>a</sup>, Leilei Wei<sup>d</sup>, Yansong Ma<sup>e</sup>, Pu-Ting Dong<sup>f</sup>, Batbileg Bor<sup>f,g</sup>, Jeffrey S. McLean<sup>h,i</sup> , Yunjie Chang<sup>j,k</sup>, Wenyuan Shi<sup>f</sup>, Lujia Cen<sup>f</sup>, Miaomiao Wu<sup>b</sup>, Jun Liu<sup>l</sup> , Yan Li<sup>b,2</sup> , Xuesong He<sup>f,g,2</sup> , and Shuai Le<sup>a,2</sup>

Edited by Nancy Moran, The University of Texas at Austin, Austin, TX; received November 10, 2023; accepted February 21, 2024

Bacteriophages (phages) play critical roles in modulating microbial ecology. Within the human microbiome, the factors influencing the long-term coexistence of phages and bacteria remain poorly investigated. Saccharibacteria (formerly TM7) are ubiquitous members of the human oral microbiome. These ultrasmall bacteria form episymbiotic relationships with their host bacteria and impact their physiology. Here, we showed that during surface-associated growth, a human oral Saccharibacteria isolate (named TM7x) protects its host bacterium, a *Schaalia odontolytica* strain (named XH001) against lytic phage LC001 predation. RNA-Sequencing analysis identified in XH001 a gene cluster with predicted functions involved in the biogenesis of cell wall polysaccharides (CWP), whose expression is significantly down-regulated when forming a symbiosis with TM7x. Through genetic work, we experimentally demonstrated the impact of the expression of this CWP gene cluster on bacterial–phage interaction by affecting phage binding. In vitro coevolution experiments further showed that the heterogeneous populations of TM7x-associated and TM7x-free XH001, which display differential susceptibility to LC001 predation, promote bacteria and phage coexistence. Our study highlights the tripartite interaction between the bacterium, episymbiont, and phage. More importantly, we present a mechanism, i.e., episymbiont-mediated modulation of gene expression in host bacteria, which impacts their susceptibility to phage predation and contributes to the formation of “source-sink” dynamics between phage and bacteria in biofilm, promoting their long-term coexistence within the human microbiome.

TM7x | Saccharibacteria | phage resistance | bacteria-phage interaction | episymbiosis

Phages are viruses that infect bacteria and play an important role in shaping community structure and impacting microbial ecology and evolution (1–3). Multiple molecular mechanisms have evolved as a result of the phage–bacterial arms race to regulate the dynamic interaction between these two antagonistic microbial entities (4, 5). These mechanisms include modifications/mutation of phage receptors on the bacterial surface to prevent phage binding (6), restriction–modification (RM) systems (7), and CRISPR-Cas adaptive immune systems to prevent phage infection by degrading intracellular phage genomes (8), bacteriophage exclusion (9, 10), Prokaryotic Argonautes-based phage defense (11), as well as recently described cyclic oligonucleotide-based antiphage signaling system (12), bacterial gasdermin systems (13), and Retron antiphage defense (14). Phages have also evolved diverse counterdefense strategies to coexist with bacteria. For example, phage can bind to mutated/modified receptors by mutating its receptor-binding proteins or evade bacterial RM system via becoming methylated by host methyltransferase upon entry (15, 16).

Most phage-resistance mechanisms are investigated in the context of single phage–bacterial host pairs (4). Accumulating evidence suggests that ecological factors of biotic or abiotic nature, such as niche spatial heterogeneity (17), local microenvironment (18), quorum sensing (19, 20), and interspecies competitions (21), may impact the dynamics of these antagonistic partners. Within the human microbiome, there are diverse microbial interspecies interactions, ranging from mutualism and commensalism to parasitism (22, 23). These interactions could profoundly impact bacterial physiology and modulate the bacterial–phage interaction (21). In this study, we presented a phage-resistance mechanism, which is achieved through an episymbiont-mediated modulation of gene expression in host bacteria and impacts the susceptibility of host bacteria to phage predation.

Saccharibacteria (formerly TM7) are ubiquitous members of the human oral microbiome yet recalcitrant to cultivation. Previously, we isolated the first Saccharibacteria strain, *Nanosynbacter lyticus* type strain TM7x (24). It exhibits a remarkably compact genome and an extraordinarily small cell size. TM7x lives as an obligate bacterial parasite on the surface

## Significance

The factors influencing the interaction between phages and bacteria, as well as their long-term coexistence, remain poorly investigated within the human microbiome. In this study, we presented a phage-resistance mechanism, which is achieved through an episymbiont-mediated modulation of gene expression in host bacteria, thus affecting their susceptibility to phage predation. More significantly, our study demonstrated that through modulating its host bacteria susceptibility to phage predation, oral episymbiont

Saccharibacteria promotes the long-term coexistence of its host bacteria and phage within the human oral microbiome by creating a “source-sink” dynamic between these two antagonistic microbial entities.

Author contributions: Y.L., X.H., and S.L. designed research; Q.Z., B.L., Jiazen Liu, W. Shen, J.W., L.W., Y.M., P.-T.D., Y.C., L.C., M.W., and Jun Liu, performed research; J.S.M. contributed new reagents/analytic tools; Q.Z., B.L., Jiazen Liu, W. Shen, J.W., L.W., Y.M., P.-T.D., B.B., J.S.M., Y.C., W. Shi, L.C., M.W., Jun Liu, Y.L., X.H., and S.L. analyzed data; and Q.Z., B.L., Jiazen Liu, W. Shen, Y.L., X.H., and S.L. wrote the paper.

The authors declare no competing interest.

This article is a PNAS Direct Submission.

Copyright © 2024 the Author(s). Published by PNAS. This open access article is distributed under Creative Commons Attribution-NonCommercial-NoDerivatives License 4.0 (CC BY-NC-ND).

<sup>1</sup>O.Z., B.L., and J.L. contributed equally to this work.

<sup>2</sup>To whom correspondence may be addressed. Email: feifeiliyan@163.com, xhe@forsyth.org, or leshuai2004@tmu.edu.cn.

This article contains supporting information online at <https://www.pnas.org/lookup/suppl/doi:10.1073/pnas.2319790121/-DCSupplemental>.

Published April 9, 2024.

of its host bacterium, *Schaalia odontolytica*, strain XH001 (formerly *Actinomyces odontolyticus* strain XH001) and impacts its physiology and pathogenesis (25). Our studies showed that the episymbiosis between XH001 and TM7x represents one of the most intriguing and likely common interspecies interactions within the human oral microbiome (26). Recently, we isolated from the human oral cavity a lytic phage LC001 that targets surface-grown, but not planktonic XH001 cells (27). Here, we showed that when forming episymbiosis with XH001, TM7x protects the surface-grown host bacteria from phage predation. This is achieved through TM7x-mediated transcriptional downregulation of a cell wall polysaccharides (CWP) biogenesis gene cluster in the host, leading to a phage-binding deficient phenotype. RNA-Seq (RNA-Sequencing) revealed a downregulated expression of this CWP gene cluster in planktonic XH001 compared to surface-grown cells, which may explain its LC001-resistance phenotype. This is further corroborated by the finding that the overexpression of this CWP gene cluster in XH001 confers LC001-binding phenotype and enhanced phage susceptibility even when grown as planktonic cells, thus strongly suggesting that this CWP gene cluster is required for phage receptor biogenesis. Most importantly, our data demonstrated that the planktonic and biofilm modes of growth, as well as its association with TM7x, modulate XH001's sensitivity to LC001 predation. The coexistence of TM7x-associated and TM7x-free XH001 subpopulations with different growth modes within the oral microbiome may affect XH001–LC001 interaction dynamics with ecological consequence.

## Results

**Episymbiont TM7x Protects Host Bacteria from Phage Predation.** Previously, we isolated from the human oral cavity a lytic phage LC001 that belongs to the Siphoviridae family and infects *S. odontolytica* XH001 efficiently and forms clear plaques in the double-layer agar plates (27). XH001 serves as the host bacterium for TM7x, an oral Saccharibacteria strain that can establish episymbiosis with XH001 (24). Culture derived from TM7x/XH001 symbiosis (termed TM7x/XH001 coculture, or coculture for short) is heterogeneous and composed of both TM7x-attached as well as TM7x-free XH001 subpopulations (28). Intriguingly, we found that the addition of LC001 to the TM7x/XH001 coculture did not induce noticeable plaque formation in the double-layer agar plates (Fig. 1A), suggesting that episymbiont TM7x may protect XH001 from LC001 predation.

Since the phage predation can be intervened at multiple steps along the infection cycle, including adsorption, genome injection, virion replication/assembly, and progeny release, we first used the adsorption assay to determine the binding of LC001 to cells collected from surface-grown XH001 and TM7x/XH001 coculture. Our data showed that compared to XH001 which displayed a high adsorption percentage (over 90%) to LC001, TM7x/XH001 cells showed a significantly decreased adsorption of under 20% (Fig. 1B). Using SYBR Green-tagged LC001, we demonstrated that phage bound effectively to XH001 cells but was defective in binding to TM7x-attached XH001 (Fig. 1C). This was further confirmed by cryoelectron tomography (cryo-ET) and transmission electron microscopy (TEM) which showed the binding of LC001 to surface-grown XH001 cells, while LC001 failed to bind and infect TM7x-associated XH001 cells (Fig. 1D and *SI Appendix*, Fig. S1).

**TM7x Episymbiosis-Induced Phage Resistance in XH001 Is Transient, Not Due to Genetic Mutation.** We next investigated whether the TM7x-mediated phage-resistant phenotype of XH001 is due to genetic mutation induced by episymbiosis

with TM7x. We first streaked TM7x/XH001 coculture on the agar plate. TM7x-attached XH001 single colonies as indicated by their irregular colonies morphology as described previously (28), were picked and grown in fresh medium to develop into a heterogeneous culture containing both TM7x-attached and TM7x-free XH001 cells as previously reported (28). This was done to ensure TM7x-free XH001 in the coculture were all derived from TM7x-attached XH001 single cells. We then further streak-isolated 3 TM7x-free XH001 colonies from the TM7x/XH001 coculture based on their reported regular colony morphology (28) (Fig. 2A). The absence of TM7x was confirmed by PCR (Fig. 2B) from cultures derived from TM7x-free XH001 colonies. Our data further showed that the surface-grown TM7x-free XH001 cells derived from TM7x-attached XH001 can be adsorbed by LC001 (Fig. 2C), and were sensitive to phage predation (Fig. 2D). These results indicated that TM7x episymbiosis does not induce phage-resistant genetic mutation in XH001, but rather, the TM7x-induced phage resistance is transient and likely through modulating the expression of XH001 function related to phage adsorption.

### TM7x Induces Downregulation in Host Bacterium XH001 of a Gene Cluster Encoding Predicted Functions Involved in CWP Biogenesis.

To further characterize the impact of TM7x on the host, we performed RNA-Seq to identify the differentially expressed genes (DEGs) between the surface-grown XH001 and TM7x/XH001 (Fig. 3A and B). A principal component analysis (PCA) and heatmap showed that the gene expression pattern of XH001 as monoculture and forming symbiosis with TM7x were very different, and within each condition, the replicates were very similar. In total, 335 genes in XH001 were differentially regulated (with 145 genes up-regulated and 190 down-regulated) upon TM7x episymbiosis (*P*-value of <0.05,  $|\log_2\text{FoldChange}| > 1$ ) (Fig. 3C). A total of 71 XH001 genes were down-regulated more than threefold in TM7x/XH001. The most down-regulated genes included those encoding Uridine diphosphate (UDP)-phosphate galactose phosphotransferase (APY09\_00485), TetR family transcriptional regulator (APY09\_06000), ABC transporter (APY09\_06050, APY09\_06055), peptidase (APY09\_09670), and cell wall-binding protein (APY09\_09665).

We further analyzed the overall changes in functional pathways based on eggNog\_COG categories (Fig. 3D). Specifically, compared to XH001, TM7-associated XH001 cells displayed a higher number of overexpressed genes than underexpressed genes in functional pathways including inorganic ion transport and metabolism; translation; replication and repair; and signal transduction. Conversely, in the functional pathways related to cell cycle; nucleotide metabolism and transport; carbohydrate metabolism and transport; coenzyme metabolism; and cell wall/membrane/envelope biogenesis, the number of genes with increased expression is lower than that with reduced expression in TM7-associated XH001 compared to XH001 cells. The data are overall consistent with our previous physiological studies which consistently demonstrated a reduced growth rate in TM7-associated XH001 compared to XH001.

Intriguingly, a gene cluster (APY09\_00485-00540) with predicted functions involved in gram-positive bacteria CWP biosynthesis was significantly down-regulated in XH001 when forming symbiosis with TM7x (Fig. 3E). An operon (APY09\_00515-APY09\_00540) was predicted using Operon-mapper (29) (Fig. 3E). Many predicted functions within the cluster are related to CWP biosynthesis, such as UDP-phosphate galactose phosphotransferase (APY09\_00485), glycosyl transferase WecB/TagA/CpsF family protein (APY09\_00490), galactose oxidases (APY09\_00500/00495), heteropolysaccharide repeat unit export protein (APY09\_00505),

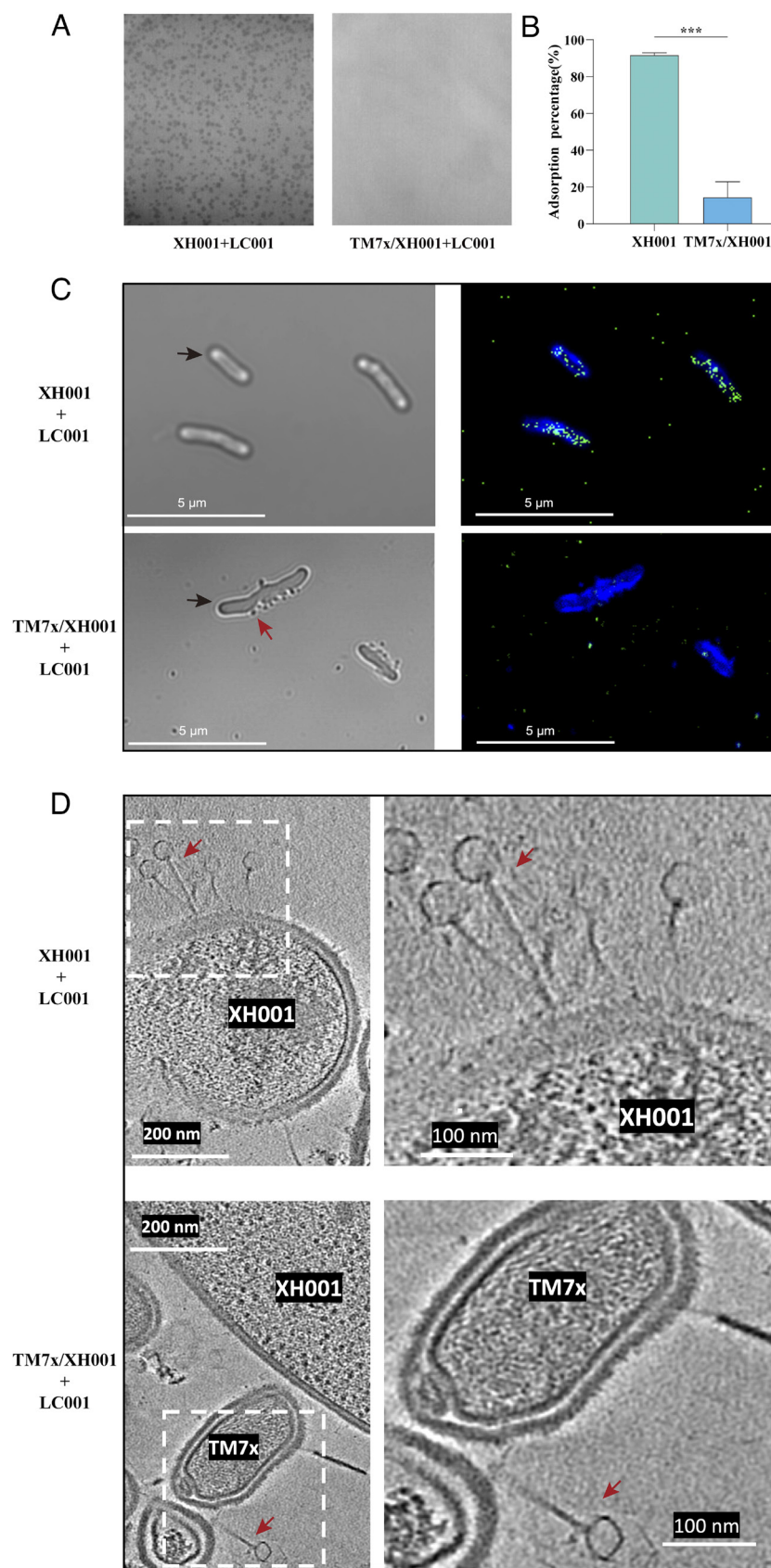


**Fig. 1.** TM7x protects host bacteria from phage predation. (A) Plaque assay of LC001 infecting *S. odontolytica* strain XH001 and TM7x/XH001. (B) The phage LC001 adsorption percentage of surface-grown XH001 and TM7x/XH001. The asterisks mark  $P$ -value of  $<0.05$  as calculated by Student's  $t$  test. (C) Microscopic observation of binding between SYBR Green-tagged LC001 and Laurdan-labeled XH001 or TM7x/XH001. The black and red arrows indicate XH001 and TM7x cells, respectively. (D) The surface-grown bacteria of XH001 or TM7x/XH001 were mixed with phage LC001 for 10 min, and the mixture was observed using the cryo-ET. The box with the dashed line indicates the area that was enlarged for closer observation of the interaction between phage LC001 and XH001. The red arrows indicate the phage LC001.

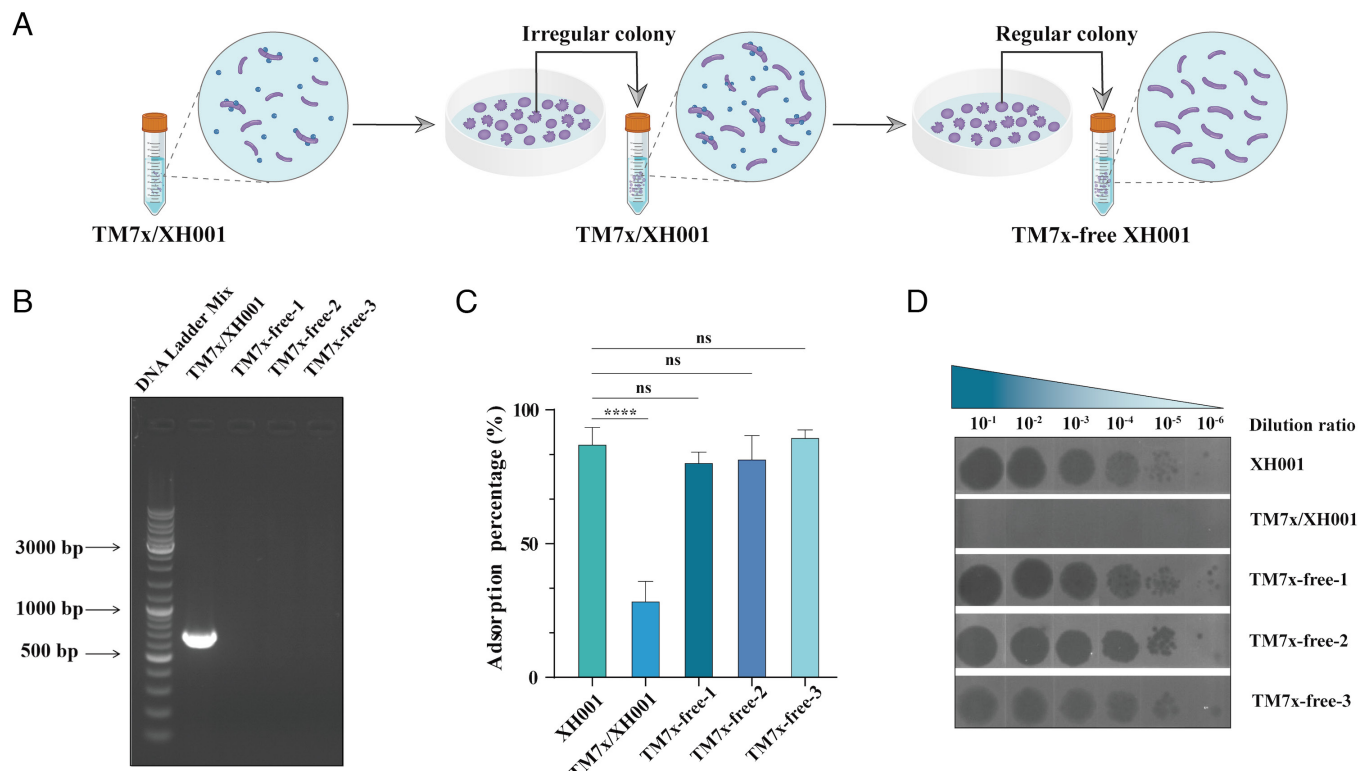


**Fig. 2.** TM7x-free XH001 derived from TM7x-associated XH001 is sensitive to phage LC001. (A) Schematic showing the isolation of TM7x-free XH001 cells from TM7x/XH001 coculture. (B) TM7x-free XH001 cells were identified by PCR using primers specific for TM7x. (C) The phage LC001 adsorption percentage for surface-grown bacteria of XH001, TM7x/XH001, and TM7x-free XH001. The asterisks mark *P*-value of <0.05 as calculated by one-way ANOVA. (D) Plaque assay of LC001 infecting XH001, TM7x/XH001, and three TM7x-free XH001 isolates.

and ligase/peptidoglycan glycosyltransferase (APY09\_00515) (30–32). Specifically, APY09\_00540, 00535, and 00530 encode glycerol-3-phosphate cytidylyltransferase, CDP-alcohol phosphatidyltransferase, and polypeptide N-acetylgalactosaminyltransferase, with predicted functions similar to TagD, TagF, and TagN, respectively, as described in *Staphylococcus aureus* PS187 (33). TagD, TagF, and TagN are responsible for synthesizing the glycerol-phosphate (GroP) repeats substituted with N-acetyl-galactosamine (GlaNAc), one of the key components of cell wall-anchored wall teichoic acids (WTA) in gram-positive bacteria (34). CWPs are abundant in gram-positive bacteria and are the typical receptors for phages (32). GlaNAc substituent on GroP repeats has been shown to be a preferred binding moiety for Siphoviridae phages targeting gram-positive bacteria (34). The positive correlation between the downregulation of this CWP gene cluster and the phage-binding defective phenotype of TM7x-associated XH001 suggests LC001 relies on CWP for successful binding and effective predation. Our data indicate that TM7x may protect XH001 from phage infection by down-regulating the expression of the CWP gene cluster.

The global shift in gene expression encompassing diverse functional pathways as revealed by transcriptomics indicated significant changes in XH001 physiology induced by TM7x. Some of the pathways could directly or indirectly affect XH001 CWP biogenesis, thus ultimately affecting XH001 sensitivity to LC001. At present, we have yet to identify the molecular mechanisms underlying how TM7x affects CWP gene clusters, an open question that warrants further investigation.

**Overexpression of the CWP Gene Cluster Renders XH001 Sensitive to Phage LC001 Predation Even When Forming Episymbiosis with TM7x.** To experimentally test the contribution of this CWP gene cluster to the infectivity of phage, the impact on phage–bacterium

interactions of this gene cluster, particularly APY09\_00540-00515, which are in the same predicted operon, was assessed using the XH001 strain in which these genes are overexpressed. As detailed in *Materials and Methods*, a strong promoter of the Kan<sup>R</sup> gene, which has been shown to function in XH001, was cloned from plasmid pJRD215 (27) and inserted upstream of APY09\_00540 to generate a CWP gene cluster overexpression strain named XH001::CWP (Fig. 4*A*). Our qRT-PCR analysis showed a significantly increased expression of APY09\_00540-00515 in XH001::CWP compared to XH001 (*SI Appendix*, Fig. S2). The XH001::CWP strain was then used to form episymbiosis with TM7x as previously described (28), and the resulting symbiosis was named TM7x/XH001::CWP. Choosing APY09\_00540 as a representative gene of the CWP cluster, qRT-PCR data showed that overexpression of CWP restored the gene expression of APY09\_00540 in TM7x/XH001::CWP to a similar level in surface-grown XH001 (Fig. 4*B*).

We then investigated whether the overexpression of CWP may impact the phage sensitivity of XH001 when it forms episymbiosis with TM7x. Our data showed that as revealed by a fluorescence microscope using SYBR Green-tagged LC001, overexpression of CWP led to significantly enhanced phage binding to surface-grown XH001 cells even when they formed episymbiosis with TM7x (Fig. 4 *C* and *D*). Furthermore, unlike TM7x/XH001, TM7x/XH001::CWP becomes sensitive to LC001, displaying an efficiency of plating (EOP) similar to that of surface-grown wildtype XH001 (Fig. 4*E*). TEM also confirmed that LC001 was able to bind to XH001::CWP cells even when they formed episymbiosis with TM7x (Fig. 4*F*). As a control, we showed that LC001 failed to bind and infect TM7x-associated XH001 cells (Fig. 4 *D–F*). These data imply that this gene cluster, particularly APY09\_00540-00515, contributes to the infectivity of LC001 by facilitating phage binding.

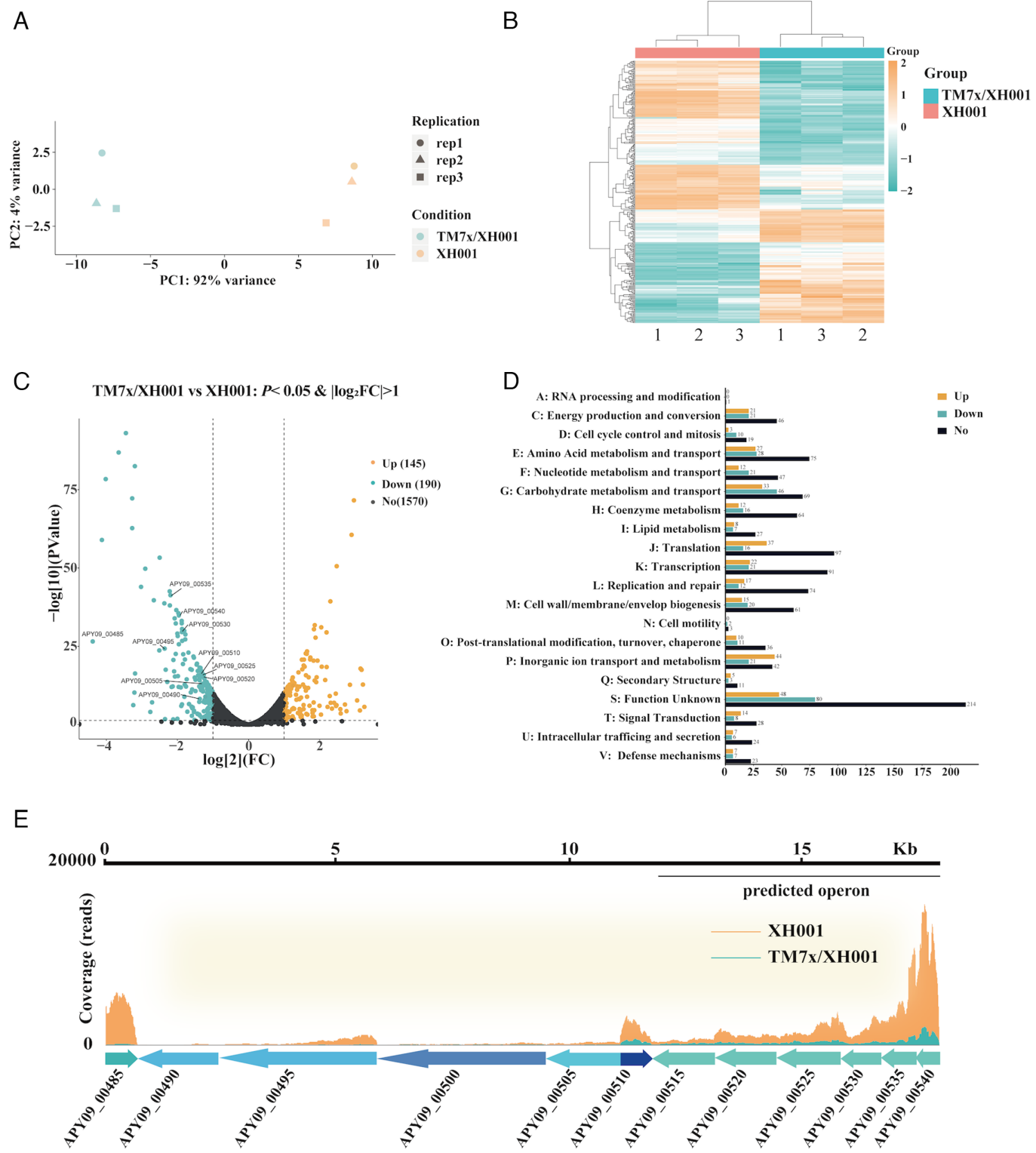


**Fig. 3.** Transcriptomic analysis of surface-growth XH001 and TM7x/XH001. (A) The transcriptomic data were subjected to PCA. The abscissa is the first principal component, and the ordinate is the second principal component. Green and orange dots represent samples of TM7x/XH001 and XH001, respectively, with three biological replicates for each group. (B) The DEGs between TM7x/XH001 and XH001 were grouped and clustered. Genes and samples were represented horizontally and vertically, respectively. Orange indicates highly expressed genes, and green indicates lowly expressed genes. (C) The volcano plot shows the gene expression levels of TM7x/XH001 compared to XH001. The threshold is set for  $P$ -value  $< 0.05$  and  $|\log_2(\text{FoldChange})| > 1$ . Orange and green dots indicate significantly up-regulated and down-regulated genes, respectively, and black dots indicate genes with no significant changes. (D) Clusters of orthologous groups (COG). The number of unchanged (black) and significantly differentially expressed (colored) genes in TM7x/XH001 vs. XH001 for each COG is shown. (E) Overall genome arrangement of the putative *S. odontolytica* CWP gene cluster. The orange and green peaks represent the APY09\_00485-540 gene expression levels in the surface-grown XH001 and TM7x/XH001, respectively.

**The Downregulation of CWP in Planktonic XH001 Prevents Phage Adsorption and Infection.** Previously, we reported that LC001 only infects the surface-grown, but not planktonic, XH001 (27). Thus, RNA-Seq was performed to compare the DEGs between the

surface-grown and the planktonic XH001 to determine whether the CWP cluster is potentially involved. Our transcriptomic data showed that 872 genes were differentially expressed in XH001 between surface and planktonic growth conditions ( $P$ -value of

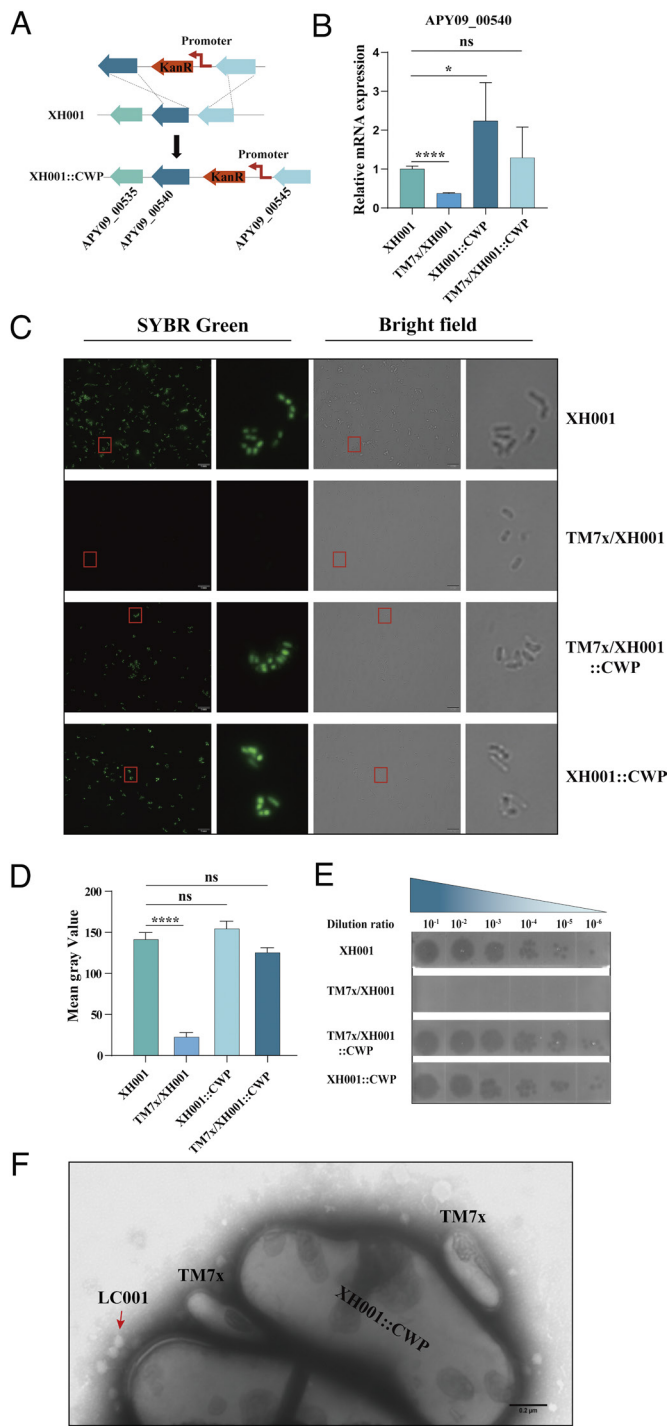


**Fig. 4.** The impact of the expression of CWP cluster in XH001 on its phage LC001 sensitivity. (A) Schematic map showing generation of XH001::CWP using homologous recombination in XH001. (B) The relative mRNA expression of APY09\_00540 was detected by qRT-PCR. The asterisks mark *P*-value of <0.05 as calculated by Student's *t* test. (C) The surface-grown bacteria of XH001, TM7x/XH001, TM7x/XH001::CWP, or XH001::CWP were mixed with the SYBR Green-labeled phage LC001 for 10 min, and the mixture was observed using the fluorescence microscope intermediately. (D) The mean fluorescence intensity of LC001 adsorbed by XH001, TM7x/XH001, TM7x/XH001::CWP, or XH001::CWP was determined by ImageJ software. The asterisks mark *P*-value of <0.05 as calculated by one-way ANOVA. (E) Plaque assay of LC001 infecting XH001, TM7x/XH001, TM7x/XH001::CWP, or XH001::CWP. (F) The surface-grown bacteria of TM7x/XH001::CWP were mixed with phage LC001 for 10 min, and the mixture was observed using the TEM. The red arrow points to the phage LC001.

<0.05,  $|\log_2\text{FoldChange}| > 1$ ) (Fig. 5A). Compared to surface-grown cells, planktonic XH001 demonstrated a higher number of genes with elevated expression in functions such as inorganic ion

transport and metabolism; amino acid metabolism and transport; carbohydrate metabolism and transport; replication and repair; and intracellular trafficking and secretion. On the other hand, planktonic XH001 exhibited a lower number of overexpressed genes in functional pathways including energy production and conversion; nucleotide metabolism and transport; translation; defense mechanisms; and cell wall/membrane/envelope biogenesis (Fig. 5B) compared to surface-grown cells.

A total of 238 XH001 genes were down-regulated more than threefold in planktonic growth, including the CWP gene cluster (Fig. 5C), suggesting that the downregulation of CWP could contribute to the phage-resistance phenotype of planktonic XH001, similar to TM7x-associated XH001. The involvement of CWP in phage binding is further confirmed by the observed LC001-sensitive phenotype in planktonic XH001::CWP strain where the CWP cluster, particularly APY09\_00540-00515 genes, is up-regulated by the introduced Kan<sup>R</sup> promoter.

We then interrogated whether CWP expression impacts XH001 phage sensitivity by affecting LC001 binding. Our data showed that when the CWP gene cluster was up-regulated, the XH001::CWP strain could be adsorbed by phage LC001 in both surface-grown and planktonic statuses. In contrast, LC001 could not adsorb to the planktonic XH001 cells (Fig. 5 D and E), further confirming the vital role of the CWP gene cluster in contributing to phage binding.

**The Heterogeneous Population of XH001 Promotes XH001 and LC001 Coexistence.** Through an evolutionary arms race and fluctuating selection dynamics, bacteria and phages continuously and reciprocally select for alterations in either bacterial antiviral defenses or viral infectivity in response to an adaptation by their counterpart in a bid to ensure their survival (35). The phage–bacteria coevolution in the context of oral microbiome is poorly investigated (36, 37). The coculture of planktonic TM7x/XH001 maintains a reservoir of a small subpopulation of TM7x-free XH001 cells (28). When incubated in a test tube under static conditions, planktonic XH001 or TM7x/XH001 culture always contains both planktonic (stay resuspended) and surface-associated (stay precipitated and aggregated) cells, which displayed differential sensitivity to phage LC001 infection as shown above. Thus, we hypothesize that the coexistence of phage-susceptible and resistant subpopulations of XH001 may continuously support phage replication and promote long-term coexistence between phages and bacteria.

We mixed phage LC001 with XH001 or TM7x/XH001 in the test tubes and subjected them to static incubation. One-tenth of the volume of the culture (after mixing) was transferred to a fresh liquid culture medium every 48 h for 10 successive passages (Fig. 6A) with three biological repeats. Interestingly, the numbers of bacterium XH001 and phage LC001 remained relatively stable over the 10 passages, with phage titer varying between  $10^7$ – $10^9$  Plaque-Forming Unit (PFU) /mL (Fig. 6 B and C). This indicates that LC001 could coexist with XH001 or TM7x/XH001 in this experiment model.

In previous reports, lytic phage–bacteria–host interactions led to the arms race in the beginning, which means the evolved phage could infect the unevolved bacteria, and the evolved bacteria resist more phages from the previous time points (38, 39). To test whether phage and bacteria coevolve, we isolated nine phages (three from each biological replication) and nine colonies (three from each biological replication) of XH001 or TM7x-free XH001 from the original XH001 monoculture and TM7x/XH001 coculture, respectively, from each timepoint at passage 0 (T0), passage 5 (T5), and passage 10 (T10). Then, we performed the classical cross-infection experiment (38).

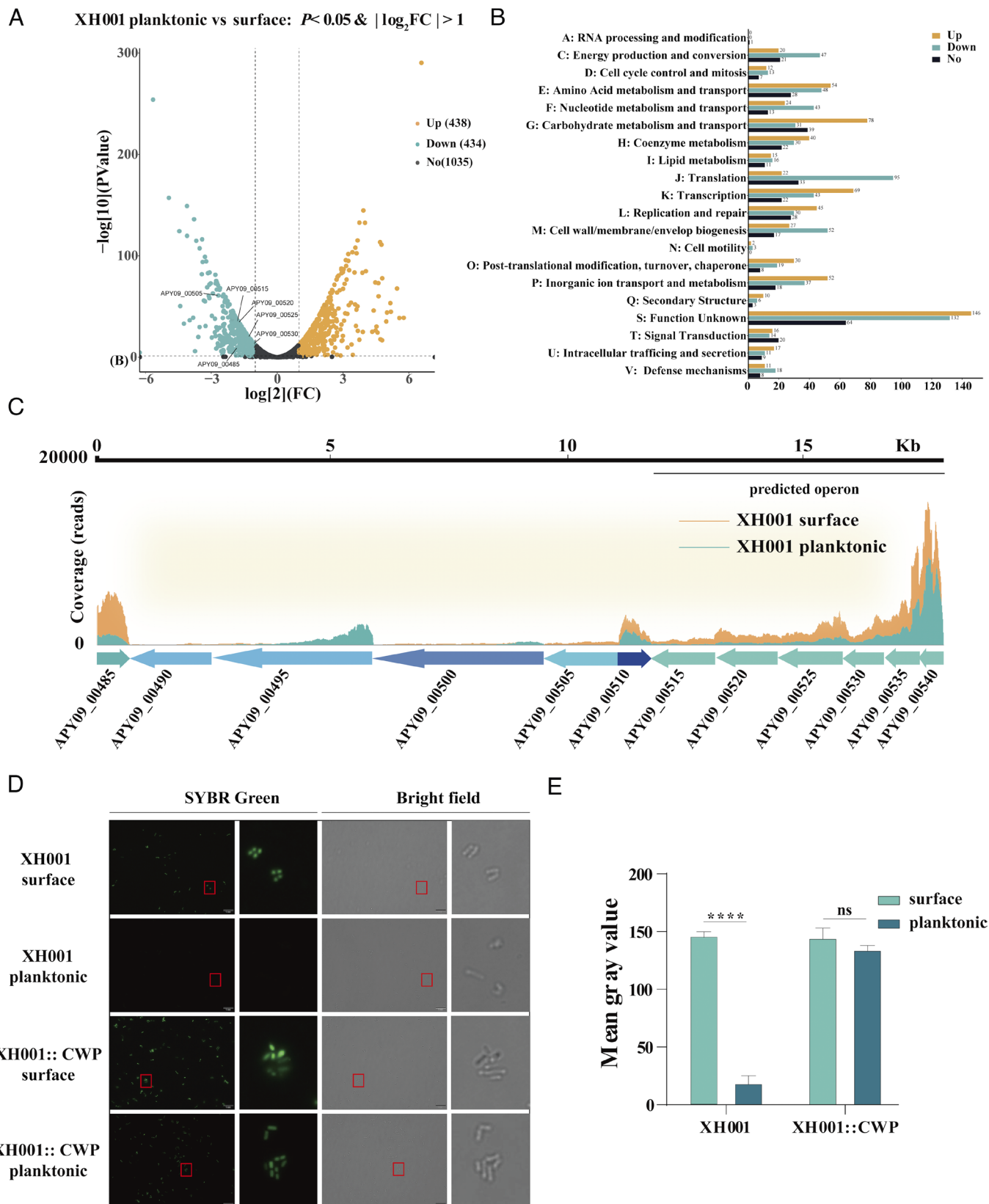


**Fig. 5.** Transcriptomic analysis of surface-grown and planktonic XH001. (A) The volcano plot shows the DEGs under the surface and planktonic growth of XH001. The threshold is set for  $P$ -value of  $<0.05$  and  $|\log_2 \text{FoldChange}| > 1$ . Orange and green dots indicate significantly up-regulated and down-regulated genes, respectively, and black dots indicate genes with no significant changes. (B) Clusters of orthologous groups (COG). The number of unchanged (black) and significantly differentially expressed (colored) genes in planktonic vs. surface-grown XH001 for each COG is shown. (C) Overall genome arrangement of the *S. odontolytica* CWP gene cluster. The orange and green peaks represent the APY09\_00485-540 gene expression levels of XH001 under surface and planktonic growth, respectively. (D) The surface and planktonic growth bacteria of XH001 or XH001::CWP were mixed with the SYBR Green-labeled phage LC001 for 10 min, and the mixture was immediately observed using the fluorescence microscope. (E) The mean fluorescence intensity of LC001 adsorbed by XH001 or XH001::CWP under surface and planktonic growth. The asterisks mark  $P$ -value of  $<0.05$  as calculated by two-way ANOVA.

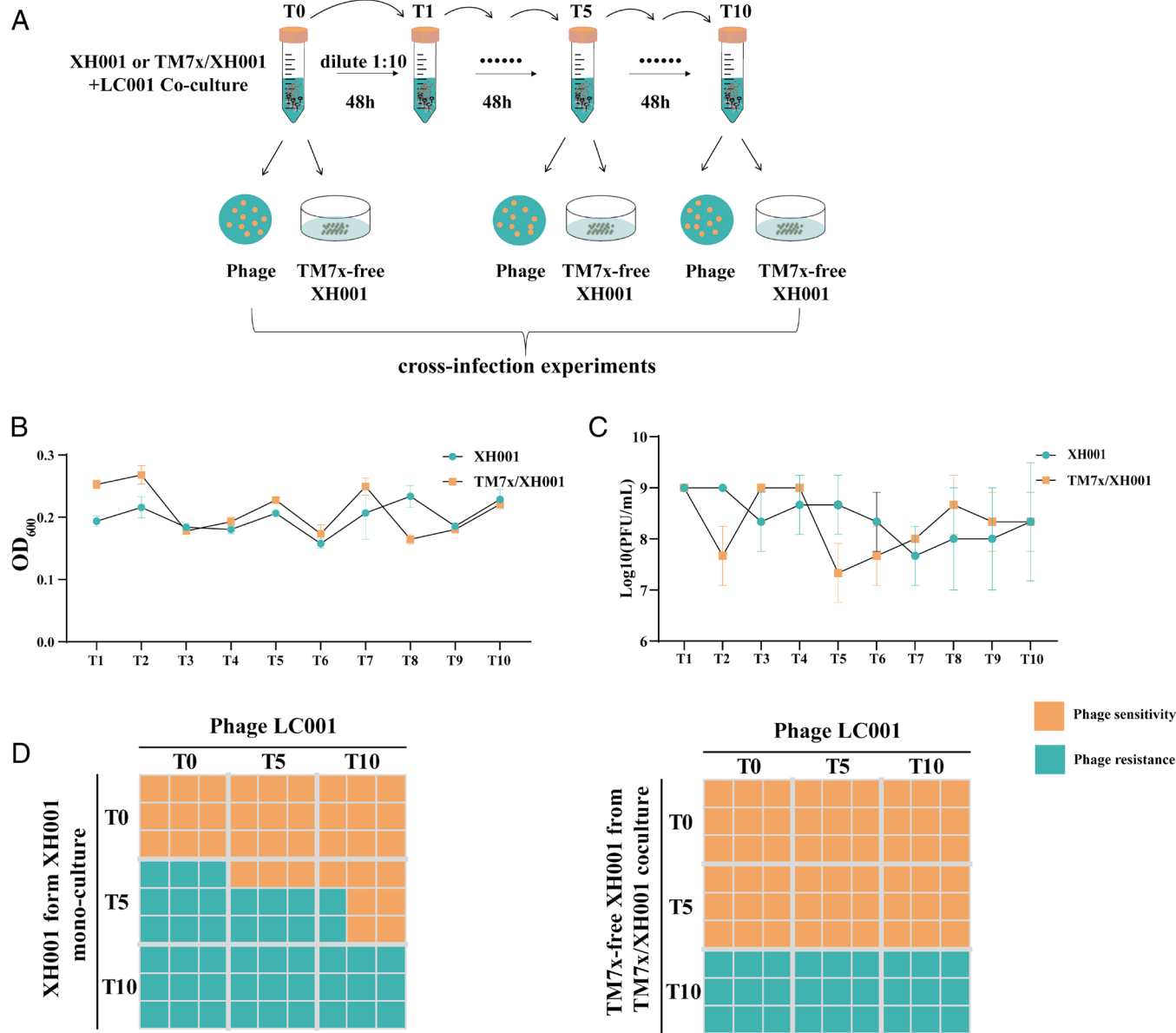


**Fig. 6.** In vitro bacteria and phage coevolution experiment. (A) Phage LC001 was cocultured with XH001 or TM7x/XH001 in liquid culture, and 1/10 volume of the coculture was transferred to a fresh Brain Heart Infusion (BHI) medium for 10 passages. The bacterial density was calculated by measuring the optical density (OD) at 600 nm, and the supernatant containing LC001 was harvested to detect the PFU of the phage. XH001, TM7x-free XH001, and phage LC001 at transfer 0, 5, and 10 were isolated and purified, and cross-infection experiments were used to test whether the isolated phages were able to infect hosts from the coevolved populations. (B) The OD<sub>600</sub> of bacteria showed that the number of hosts in both of the coevolved populations remained stable. (C) Phage titer in each generation was measured by the EOP experiment using the wild-type XH001 as a host, which showed that the phage population was maintained in both of the coevolved populations. (D) The phage infectivity range is based on the ability of each isolated phage to infect 3 XH001 or TM7x-free XH001 clones from the host population of T0, T5, and T10. Infection by phage is marked in orange, and resistance by hosts is marked in green. The phage infectivity range indicates an arms race model between XH001 and LC001, while TM7x delays the coevolution of phage and bacterial populations.

We showed that in the XH001–LC001 setup, phages isolated at T0 failed to infect any of the XH001 isolated from T5 or T10 (Fig. 6D), suggesting that by T5, the XH001 population has already evolved to become resistant to T0 phages. Phages from T10 displayed their infectivity against seven out of the nine XH001 isolates from T5, suggesting that phage is evolving, indicating the ongoing arms race. For the TM7x/XH001–LC001 setup, the arms race was also observed but at a slower pace than that in the XH001–LC001 group. All the TM7x-free XH001 isolated from T5 were susceptible to all the phages, including those isolated from T0 (Fig. 6D), indicating that bacteria had not evolved by T5. However, by T10, all the TM7x-free XH001 isolated resisted all the phages, suggesting that the phage-resistant TM7x-free XH001, which evolved as a result of the arms race,

might have an advantage and dominate the population under this specific in vitro setting.

## Discussion

Multiple molecular mechanisms regulate the dynamics of phage–bacterium interactions (4). However, in the context of host-associated microbiome, how the extensive bacterial interspecies interactions may impact the bacterial–phage ecology and evolution remains poorly understood (1). In this study, we demonstrated the differential phage susceptibility displayed by an oral bacterial species *S. odontolyticus* strain XH001 under different growth modes: surface-grown vs. planktonic and free-living vs. forming symbiosis with episymbiont TM7x. The coexistence of

these XH001 subpopulations within the microbial community may not only offer an episymbiont-mediated phage-resistance mechanism protecting XH001 within biofilm from being eradicated by lytic phage but also present a mechanism to promote the long-term coexistence of the lytic phage LC001 and bacterium XH001 within the oral cavity, which is of ecological significance.

We first revealed the differential sensitivity to phage LC001 predation exhibited by XH001 during different growth modes, e.g., surface-grown XH001 is sensitive to LC001, while it becomes phage resistant during planktonic growth or forming symbiosis with TM7x. We further identified in XH001 a CWP gene cluster with predicted functions involved in WTA biosynthesis. Its expression is positively correlated with bacterial affinity to phage LC001 binding and its sensitivity to LC001 predation. The involvement of this CWP gene cluster in mediating LC001 binding was further experimentally confirmed by constitutive expression, which led to a phage-sensitive phenotype regardless of its growth modes (Figs. 4 and 5).

Bacteria, particularly gram-positive bacteria such as XH001, possess an extraordinary repertoire of CWPs with critical physiological functions, which are the main virulence factors of pathogens. The CWP is the essential structure that protects a bacterium from and interacts with its surrounding environment (40). Ironically, these CWPs often serve as receptors for phage binding. For example, CWPs with highly variable structures among *Lactococcus lactis* strains have been identified as receptors for phages of several families (41). Among CWPs, WTAs are the most abundant peptidoglycan-linked polymers in many gram-positive bacteria (42) and are the most common receptors targeted by phages infecting gram-positive hosts (43). However, few phage receptors have been identified and characterized thus far for gram-positive bacteria due to the complexity of cell walls containing different moieties that can contribute to phage adsorption. At the moment, the exact binding moiety for phage LC001 in XH001 CWP remains to be determined. Future studies should also focus on identifying the molecular mechanism that governs how TM7x affects the expression of CWP gene clusters in XH001.

Importantly, our study found a bacterial episymbiont-mediated phage-resistance mechanism. We showed that by forming a symbiosis with epibiont *Saccharibacterium* TM7x, XH001 downregulated the CWP gene cluster, reducing phage receptors in surface-grown XH001 to prevent phage adsorption (Fig. 1). Thus even without dedicated defense systems, surface-grown XH001, may escape phage predation via episymbiont-mediated phage resistance. Intriguingly, TM7x-induced phage resistance is transient and reversible. XH001 cells lost their phage resistance when they were detached from TM7x or derived from TM7x-associated XH001 via cell division. This is reminiscent of the reported phase-variable, transient defense against phage (44, 45). Phase variation is believed to stem from the need to adapt to opposing, repetitive, fluctuating selection for or against particular traits (46), leading to changes in phage sensitivity to the host (47). For example, phase variably expressed O-antigen glucosylating gene cluster would lead to the  $\alpha$ -1,4-glucosylation of galactose residues in the O12-antigen of *Salmonella Typhimurium* to prevent phage adsorption. Phages can also adapt to host changes dependent on a phase-variable receptor. It has been reported that the Fletchervirus phages mimic their host and encode hypermutable polyG tracts, leading to phenotypically diverse and infectious phage populations (48). However, the previously reported phase variation occurs with a relative frequency ranging from  $10^{-4}$  to  $10^{-1}$  per generation with various molecular mechanisms (site-specific recombination, differential DNA methylation, and slipped-strand mispairing) (49–51), while episymbiont

TM7x-induced phase resistance is much more effective, as reflected by the absence of plaque formation when TM7x/XH001 coculture was challenged with LC001. This is due to TM7x-induced significant downregulation of functions involved in phage receptor biogenesis, thus conferring phage resistance. The observed episymbiont TM7x-induced phenotypic switching could be a survival strategy developed by XH001 to adapt to the changing environment and cope with phage selective pressure.

While TM7x was initially regarded as a “parasite” that negatively affects the growth of its bacterial host when forming episymbiosis with XH001 under laboratory conditions (24, 52), increasing lines of evidence indicated that association with TM7x is potentially beneficial to the host bacteria within the natural niche. For example, TM7x may protect XH001 from acidic stress via its encoded arginine deiminase system (53), as well as promote XH001 persistence within the oral cavity by enhancing biofilm formation (54). Our data provide additional evidence to highlight the benefit conferred by TM7x to its host bacteria and further emphasize the context-dependent nature of symbiotic relationships (55, 56).

Our in vitro coevolution experiments further demonstrated that when forming episymbiosis with TM7x, the heterogeneous populations of phage-sensitive TM7x-free XH001 and phage-resistant TM7x-associated XH001 cells promoted the long-term coexistence of bacteria and phage. This is reflected by the more passages needed for XH001 to evolve in TM7x/XH001 coculture compared to XH001 monoculture when challenged with phage LC001. The in vitro experimental setup we used, although classical, has many drawbacks. For example, its simplicity does not fully reflect the microenvironment with diverse ecological factors. Nevertheless, our data clearly indicated a weaker selective pressure experienced by XH001 within TM7x/XH001 coculture compared to XH001 monoculture.

It has been established that as the two antagonistic microbial entities, bacteria and phages are constantly engaged in the arms race (4) where they continuously and reciprocally select for alterations in either bacterial antiviral defenses or viral infectivity in response to an adaptation by their counterpart in a bid to ensure their survival and coexistence (1). These are often achieved through genetic mutations. However, recent studies of bacterial–phage interaction, especially in the context of host-associated microbiome indicated that ecological factors, such as niche spatial heterogeneity (17) and local microenvironment-induced gene expression regulation (18), may impact the dynamics of these antagonistic partners and promote bacteria phage coexistence without undergoing constant genetic mutation.

Within the oral cavity, due to saliva flow, bacteria that are unable to attach to the surface or fail to integrate into biofilm are constantly cleared and washed down the gastrointestinal tract. Thus, biofilm is the most dominant and relevant growth mode (26). As a commensal bacterium, XH001 is a ubiquitous constituent of oral biofilm and may be subject to constant selective pressure from lytic phages such as LC001. The formation of symbiosis with epibiont TM7x releases such pressure by becoming phage resistant. More importantly, the coexistence within the biofilm of free-living and TM7x-associated XH001 populations with differential LC001 sensitivity may create “source-sink” dynamics between the two antagonistic partners. While phage LC001 infects free-living XH001 cells, promoting phage replication (sink), TM7x-associated XH001 is resistant to and escapes LC001 predation. Via bacterial replication, the TM7x-associated XH001 subpopulation could constantly produce new TM7x-free XH001 daughter cells (source) as prey for LC001. Similar source-sink dynamics have recently been described for bacterial–phage interaction in the gut

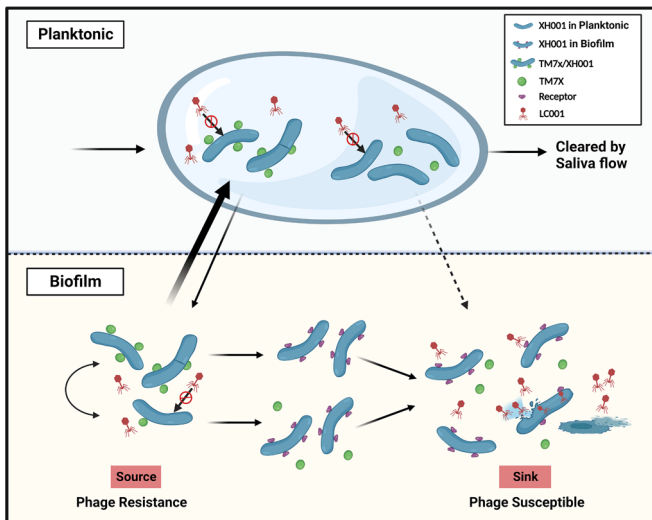


**Fig. 7.** The model of episymbiont TM7x modulates the phage resistance of its host bacteria and impacts bacterial-phage interaction dynamics. Within the oral cavity, biofilm is the most dominant and relevant growth mode. The coexistence within the biofilm of free-living and TM7x-associated XH001 populations with differential LC001 sensitivity creates source-sink dynamics between the two antagonistic partners to promote the coexistence of bacteria and phage.

microbiome, although it was achieved through spatial heterogeneity (17). In our study, source-sink dynamics result from a heterogeneous population of free-living and TM7x-associated XH001 cells with differential LC001 resistance, which contributes to long-term coexistence within biofilm without undergoing a drastic mutation-based arms race (Fig. 7).

In conclusion, we described a tripartite system involving an oral bacterium (XH001), its episymbiont (TM7x), and XH001-targeting lytic phage (LC001). Their intricate interactions modulate their physiology and biology with ecological consequences. Episymbiosis between Saccharibacteria, such as TM7x, and their bacterial hosts represents one of the most ubiquitous yet understudied interspecies interactions within the human oral microbiome. Our study thus presents a phage-resistance mechanism mediated through the formation of episymbiosis, which expands the list of mechanisms for promoting the long-term coexistence of bacteria and phage within a host-associated microbiome.

## Materials and Methods

**Bacterial Strains, Phages, and Growth Conditions.** The bacterial strains and phages in this work are listed in *SI Appendix, Table S1*. *S. odontolytica* strain XH001 was grown on brain heart infusion (BHI, Oxoid, UK) broth or 1.5% agar (Dingguo, Beijing, China) at 37 °C under microaerophilic conditions (5% O<sub>2</sub>, 5% CO<sub>2</sub>, balanced with N<sub>2</sub>). TM7x/XH001 coculture was maintained under microaerophilic conditions. Kanamycin (160 µg/mL, Fisher Bioreagents) was added to the growth medium when required for antibiotic selection. The LC001 phage was propagated on the host strain for 24 h at 37 °C in BHI under the microaerophilic conditions. The supernatants containing amplified phages were sterilized through a 0.22 µm filter and stored at -80 °C with a final glycerol concentration of 20%.

**Plaque Assay and EOP Assay.** The phage plaque assay was performed by spotting phages on bacterial soft agar overlays. Specifically, 100 µL of logarithmic-phase bacterial culture, with an OD<sub>600</sub> of 0.5, was mixed with 100 µL of diluted phage and 6 mL of 0.45% BHI agar and then overlaid onto BHI agar plates. Subsequently, the plate was incubated overnight at 37 °C under microaerophilic conditions. Once the plaques developed, they were counted, and the EOP of phages on various bacteria was calculated as previously described (57). Briefly, double-layer agar plates premixed with a host strain were spotted with 2 µL of serial 10-fold dilutions of a phage solution, followed by incubation at 37 °C under microaerophilic conditions. Phage titers were calculated after 24 h.

**Adsorption Assay.** Bacterial cells, whether cultured in liquid medium or grown on agar plates, were harvested and resuspended in BHI broth. One milliliter of host cell suspension (containing about 10<sup>9</sup> cells) was mixed with 100 µL of LC001 phage (approximately 10<sup>4</sup> phage particles), and the mixture was incubated at 37 °C for 10 min with shaking. Subsequently, the mixture was filtered through a 0.22 µm filter, and the phage count in the supernatant was calculated by the plaque assay. The phage adsorption rate was calculated using the formula [(initial phage titer – residual titer in filtrate)/initial phage titer] × 100%. Student's *t* test or one-way ANOVA was conducted to compare the binding differences between LC001 and various host cells.

**TEM.** Host cells that had grown on agar surfaces were harvested and suspended in PBS (phosphate-buffered saline) (with an OD<sub>600</sub> of 0.2). A volume of 100 µL of bacterial cells was mixed with 100 µL of LC001 solution containing a phage titer of 10<sup>10</sup> PFU/mL. The mixture was then incubated at 37 °C for 10 min. The resulting mixture was utilized for subsequent TEM and cryo-ET sample preparation. For TEM samples, 10 µL of the mixed culture was deposited onto copper grids with carbon-coated Formvar films. The grids were then dried and negatively stained with 2% phosphotungstic acid (pH 6.8). Analysis was performed using Hitachi TEM (HITACHI HT7700, Japan) equipment operating at 100 kV.

**cryo-ET.** Agar surface-grown XH001 or TM7x/XH001 cells were collected and resuspended in PBS (~10<sup>9</sup> cells/mL). A volume of 100 µL of cell solution was mixed with 100 µL of LC001 solution containing a phage titer of 10<sup>10</sup> PFU/mL and used for subsequent cryo-ET sample preparation.

Cryo-ET samples were prepared using copper grids with holey carbon support film (200 mesh, R2/1, Quantifoil) as previously described (27). The grids were glow-discharged for ~30 s before depositing 5 µL of cell solution onto them. Then, the grids were blotted with Whatman filter paper from the back side for about 8 s and rapidly frozen in liquid ethane cooled with liquid nitrogen using a homemade gravity-driven plunger apparatus.

The plunge-frozen grids were clipped into cryogenic focused ion beam (cryo-FIB) AutoGrids and mounted into the specimen shuttle under liquid nitrogen. Samples were milled to thin lamellae using an Aquilos cryo-FIB system (Thermo Fisher Scientific) as previously described. A thin Pt layer was then sputter-coated onto the lamella to prevent a possible charging issue during the cryo-ET imaging, and the grids were stored in liquid nitrogen.

The cryo-FIB lamellae were transferred to a 300 kV Titan Krios electron microscope (Thermo Fisher Scientific) that was equipped with a Direct Electron Detector, a Volta Phase Plate (VPP), and an energy filter (Gatan). SerialEM (58) was used to collect single-axis tilt series around 0 µm defocus with VPP, with a cumulative dose of ~90 e<sup>-</sup>/Å covering tilt angles from -51° to 51° (3° tilt step). Images were acquired with an effective pixel size of 3.384 Å at the specimen level. All recorded images were first drift corrected by the software MotionCor2 (59) and then stacked by the software package IMOD (60). The tilt series were then aligned by IMOD with the patching tracking method. Tomograms were then reconstructed in IMOD, using the aligned stacks. A representative section was selected from the tomograms corresponding to different samples.

## Visualizing Phage Attachment to Host Cells Using Fluorescence Microscopy

**Microscopy.** Phage adsorption to host cells was examined using the established SYBR Green-labeling method (27). Briefly, phage particles were mixed at a ratio of 1,000:1 (volume/volume) with a 10-fold-diluted SYBR Gold stock solution (Invitrogen, Waltham, MA) and incubated overnight at 4 °C in darkness. Bacterial cells were cultured overnight on BHI liquid or agar plates. Subsequently, the bacteria cells were adjusted to an OD<sub>600</sub> of 0.5 (containing 10<sup>8</sup> cells/mL) in PBS. When indicated, the cells were stained with 4 µM Laurdan (Invitrogen, Waltham, MA) for 30 min and then washed twice with Ringer's solution. Following this, bacteria were then mixed with SYBR Green-stained phages at MOIs of approximately 1:100. The mixtures were incubated at 37 °C for 10 min and visualized using fluorescence microscopy (LSM880, Zeiss, Germany) at a magnification of ×1,000. Fluorescence from SYBR Green-stained phages was detected with an excitation wavelength of 405 nm and emission in the range of 420 to 470 nm. Three biological replicates were conducted.

**RNA-Seq.** Bacteria were cultured overnight on BHI liquid or agar plates at 37 °C under the microaerophilic conditions. The bacteria were collected and then resuspended in TRIzol Reagent (Invitrogen, Carlsbad, CA), immediately frozen with

liquid nitrogen, and stored at  $-80^{\circ}\text{C}$ . Three biological repeats were performed. RNA extraction and RNA-Seq analysis were conducted following the previously described procedure (57). After eliminating rRNA using the Zymo-Seq RiboFree Total RNA Library Kit (Zymo Research, USA), cDNA libraries were constructed and sequenced on NovaSeq 6000 platform (Illumina, USA). HTSeq (v0.9.1) was used to statistically compare the read count value for each gene and DESeq (v1.38.3) was conducted to analyze the differential expressed mRNA. Differential gene expression was identified using the threshold of the parametric  $P$ -value  $< 0.05$  and  $\log_2|\text{fold change}| > 1$ .

**Quantitative Real-Time RT-PCR (qRT-PCR).** qRT-PCR was conducted as described previously (57). Bacteria were cultured overnight on BHI liquid or agar plates at  $37^{\circ}\text{C}$  under the microaerophilic conditions. Samples were collected and resuspended with TRIzol Reagent (Invitrogen, Carlsbad, CA). Total RNA was extracted and reverse transcribed with the PrimeScript<sup>TM</sup> RT Reagent Kit (TaKaRa, Japan). Then, the QuantiNova SYBR Green PCR Kit (QIAGEN, Germany) was used to run qRT-PCR on the Bio-Rad CFX96 system (Bio-Rad, USA). 16S rRNA served as an internal control, and the relative gene expression level was calculated using the  $2^{-\Delta\Delta Ct}$  formula ( $\Delta Ct = \text{Target Gene} - \text{Reference Gene}$ ).

**Generation of a CWP Overexpression Strain in XH001 through Allelic Replacement.** The XH001::CWP strain, generated in this study, was constructed and verified as previously described (27). For the construction of the XH001::CWP strain, we conducted PCR amplification and fusion of approximately 2 kb homologous fragment from both upstream and downstream regions of the APY09\_00540 transcription start site, along with a kanamycin gene resistance cassette from pJDR215 (27). The FastPure Gel DNA Extraction Mini Kit (Vazyme, Nanjing, China) was used to purify and concentrate the resulting linear fragment following the manufacturer's instructions. In order to generate sufficient product before transformation and allelic replacement, the PrimeSTAR<sup>®</sup> Max DNA Polymerase (TaKaRa, Japan) was used for PCR amplification of the resulting construct. The derivative cassette carrying the homologous fragment was then transformed into XH001. Transformants were selected on kanamycin-containing agar plates and confirmed through diagnostic PCR. The primers are listed in *SI Appendix, Table S2*.

**Isolation and Reinfection of TM7x.** The isolation and reinfection of TM7x were performed according to previous studies (24). Briefly, TM7x/XH001 coculture was centrifuged at 4,500 g for 10 min. The supernatants containing host-free TM7x cells were passed through a 0.45  $\mu\text{m}$  filter. The isolated TM7x was added in XH001::CWP, and the mixture was incubated at room temperature for 10 min before adding an extra 2 mL of fresh BHI. The culture was then incubated for 24 h in a microaerophilic chamber at  $37^{\circ}\text{C}$  and transferred to fresh media with a final concentration of  $\text{OD}_{600} = 0.1$ . Subsequently, this passaging was repeated every 24 h by transferring the culture into fresh media. During each passage, the cells were visualized using fluorescence microscopy (LSM880, Zeiss, Germany) to observe the formation of symbiosis between TM7x and XH001. The culture was then plated on

the BHI agar plate. The irregular colonies indicative of TM7x/XH001 symbiosis (28) were picked and cultured in fresh BHI medium, which were then further confirmed by diagnostic PCR to detect the presence of TM7x as previously described (28, 52).

**Coevolution Experiment.** First, 9 mL of host cultures (XH001 monoculture or TM7x/XH001 coculture) with an initial  $\text{OD}_{600}$  of 0.2 was mixed with 1 mL of phages ( $10^8$  PFU/mL) and incubated at  $37^{\circ}\text{C}$  under microaerophilic conditions for 48 h. Then, the coculture was transferred at a 1:10 dilution into fresh media for a total of 10 transfers. The  $\text{OD}_{600}$  of the coculture was measured, while the phage titer in the supernatant was determined by the EOP assay using the WT XH001 strain. Subsequently, bacteria and phages of the original, fifth, and tenth generations were isolated and used for the cross-infection experiments to detect the lysis and resistance of each phage to each bacterium (38, 61).

**Data, Materials, and Software Availability.** The RNA-Seq data are available in GenBank under accession number PRJNA1037312 (62).

**ACKNOWLEDGMENTS.** Research in this publication was supported by the National Institute of Dental and Craniofacial Research of the NIH under awards 1R01DE023810 (to X.H., J.S.M., and W. Shi), R01DE030943 (to X.H.), and 1R01DE031274 (to B.B.). The research was also partly supported by the National Natural Science Foundation of China grants: 31870167 (to S.L.) and 81991502 (to Y.L.). We thank Meng Shao for preparing cryo-ET samples with cryo-FIB at the Liu laboratory at Yale; Y.C. and Jun Liu were supported by grants R01GM124378 and R01GM110243 from National Institute of General Medical Sciences and R01AI152421 from the National Institute of Allergy and Infectious Diseases; cryo-ET data were collected at the Yale cryo-EM resources and funded in part by the NIH grant 1S10OD023603-01A1. The content is solely the responsibility of the authors and does not necessarily represent the official views of the NIH.

**Author affiliations:** <sup>a</sup>Department of Microbiology, College of Basic Medical Sciences, Key Laboratory of Microbial Engineering Under the Educational Committee in Chongqing, Army Medical University, Chongqing 400038, China; <sup>b</sup>State Key Laboratory of Oral Diseases, National Center for Stomatology, National Clinical Research Center for Oral Diseases, West China Hospital of Stomatology, Sichuan University, Chengdu, Sichuan 610041, China; <sup>c</sup>Department of Infectious Diseases, Institute for Viral Hepatitis, Key Laboratory of Molecular Biology for Infectious Diseases, Ministry of Education, the Second Affiliated Hospital of Chongqing Medical University, Chongqing 401336, China; <sup>d</sup>Department of Laboratory Medicine, Daping Hospital, Army Medical University, Chongqing 400038, China; <sup>e</sup>Department of Orthodontics, Capital Medical University, Beijing 100050, China; <sup>f</sup>Department of Microbiology, The American Dental Association Forsyth Institute, Cambridge, MA 02142; <sup>g</sup>Department of Oral Medicine, Infection and Immunity, Harvard School of Dental Medicine, Boston, MA 02115; <sup>h</sup>Department of Periodontics, University of Washington, Seattle, WA 98195; <sup>i</sup>Department of Microbiology, University of Washington, Seattle, WA 98195; <sup>j</sup>Department of Cell Biology, Zhejiang University School of Medicine, Hangzhou, Zhejiang 310058, China; <sup>k</sup>Department of Infectious Disease of Sir Run Run Shaw Hospital, Zhejiang University School of Medicine, Hangzhou, Zhejiang 310058, China; and <sup>l</sup>Department of Microbial Pathogenesis, Yale School of Medicine, New Haven, CT 06536

1. A. N. Shkporov, C. J. Turkington, C. Hill, Mutualistic interplay between bacteriophages and bacteria in the human gut. *Nat. Rev. Microbiol.* **20**, 737–749 (2022).
2. D. Piel *et al.*, Phage-host coevolution in natural populations. *Nat. Microbiol.* **7**, 1075–1086 (2022).
3. H. G. Hampton, B. N. J. Watson, P. C. Fineran, The arms race between bacteria and their phage foes. *Nature* **577**, 327–336 (2020).
4. H. Georjon, A. Bernheim, The highly diverse antiphage defence systems of bacteria. *Nat. Rev. Microbiol.* **21**, 686–700 (2023).
5. F. Tesson *et al.*, Systematic and quantitative view of the antiviral arsenal of prokaryotes. *Nat. Commun.* **13**, 2561 (2022).
6. M. Shen *et al.*, *Pseudomonas aeruginosa* MutL promotes large chromosomal deletions through non-homologous end joining to prevent bacteriophage predation. *Nucleic Acids Res.* **46**, 4505–4514 (2018).
7. R. A. Warren, Modified bases in bacteriophage DNAs. *Annu. Rev. Microbiol.* **34**, 137–158 (1980).
8. A. J. Meeske, S. Nakandakari-Higa, L. A. Marraffini, Cas13-induced cellular dormancy prevents the rise of CRISPR-resistant bacteriophage. *Nature* **570**, 241–245 (2019).
9. T. Goldfarb *et al.*, BREX is a novel phage resistance system widespread in microbial genomes. *The EMBO J.* **34**, 169–183 (2015).
10. B. W. Shen *et al.*, Structure, substrate binding and activity of a unique AAA+ protein: The BrxL phage restriction factor. *Nucleic Acids Res.* **51**, 3513–3528 (2023).
11. A. Kuzmenko *et al.*, DNA targeting and interference by a bacterial Argonaute nuclease. *Nature* **587**, 632–637 (2020).
12. K. M. Slavik, P. J. Kranzusch, CBASS to cGAS-STING: The origins and mechanisms of nucleotide second messenger immune signaling. *Annu. Rev. Virol.* **10**, 423–453 (2023).
13. A. G. Johnson *et al.*, Bacterial gasdermins reveal an ancient mechanism of cell death. *Science* **375**, 221–225 (2022).
14. C. Palka, C. B. Fishman, S. Bhattacharjee, S. A. Myers, S. L. Shipman, Retron reverse transcriptase termination and phage defense are dependent on host RNase H1. *Nucleic Acids Res.* **50**, 3490–3504 (2022).
15. J. E. Samson, A. H. Magadan, M. Sabri, S. Moineau, Revenge of the phages: Defeating bacterial defences. *Nat. Rev. Microbiol.* **11**, 675–687 (2013).
16. Y. Yang *et al.*, Development of a bacteriophage cocktail to constrain the emergence of phage-resistant *Pseudomonas aeruginosa*. *Front. Microbiol.* **11**, 327 (2020).
17. M. Lourenço *et al.*, The spatial heterogeneity of the gut limits predation and fosters coexistence of bacteria and bacteriophages. *Cell Host Microbe* **28**, 390–401.e5 (2020).
18. J. Majewska *et al.*, Evolution of the T4 phage virion is driven by selection pressure from non-bacterial factors. *Microbiol. Spectrum* **11**, e0011523 (2023).
19. Y. X. Wang, J. J. Dai, X. H. Wang, Y. Wang, F. Tang, Mechanisms of interactions between bacteria and bacteriophage mediate by quorum sensing systems. *Appl. Microbiol. Biotechnol.* **106**, 2299–2310 (2022).
20. T. Luthe, L. Kever, K. Thormann, J. Frunzke, Bacterial multicellular behavior in antiviral defense. *Curr. Opin. Microbiol.* **74**, 102314 (2023).
21. E. O. Alseth *et al.*, Bacterial biodiversity drives the evolution of CRISPR-based phage resistance. *Nature* **574**, 549–552 (2019).
22. R. J. Lamont, H. Koo, G. Hajishengallis, The oral microbiota: Dynamic communities and host interactions. *Nat. Rev. Microbiol.* **16**, 745–759 (2018).
23. A. Chevallereau, B. J. Pons, S. van Houte, E. R. Westra, Interactions between bacterial and phage communities in natural environments. *Nat. Rev. Microbiol.* **20**, 49–62 (2022).

24. X. He *et al.*, Cultivation of a human-associated TM7 phylotype reveals a reduced genome and epibiotic parasitic lifestyle. *Proc. Natl. Acad. Sci. U.S.A.* **112**, 244–249 (2015).
25. O. Chipashvili *et al.*, Episymbiotic Saccharibacteria suppresses gingival inflammation and bone loss in mice through host bacterial modulation. *Cell Host Microbe* **29**, 1649–1662.e7 (2021).
26. J. L. Baker, J. L. Mark Welch, K. M. Kauffman, J. S. McLean, X. He, The oral microbiome: Diversity, biogeography and human health. *Nat. Rev. Microbiol.* **22**, 89–104 (2024).
27. L. Cen *et al.*, Exploitation of a bacterium-encoded lytic transglycosylase by a human oral lytic phage to facilitate infection. *J. Virol.* **96**, e0106322 (2022).
28. B. Bor *et al.*, Rapid evolution of decreased host susceptibility drives a stable relationship between ultrasmall parasite TM7x and its bacterial host. *Proc. Natl. Acad. Sci. U.S.A.* **115**, 12277–12282 (2018).
29. B. Taboada, K. Estrada, R. Ciria, E. Merino, Operon-mapper: A web server for precise operon identification in bacterial and archaeal genomes. *Bioinformatics* **34**, 4118–4120 (2018).
30. M. D. Kattke *et al.*, Structure and mechanism of TagA, a novel membrane-associated glycosyltransferase that produces wall teichoic acids in pathogenic bacteria. *PLoS Pathog.* **15**, e1007723 (2019).
31. C. Weidenmaier, A. Peschel, Teichoic acids and related cell-wall glycopolymers in Gram-positive physiology and host interactions. *Nat. Rev. Microbiol.* **6**, 276–287 (2008).
32. S. Brown, J. P. Santa Maria, S. Walker Jr., Wall teichoic acids of gram-positive bacteria. *Annu. Rev. Microbiol.* **67**, 313–336 (2013).
33. V. Winstel, P. Sanchez-Carballo, O. Holst, G. Xia, A. Peschel, Biosynthesis of the unique wall teichoic acid of *Staphylococcus aureus* lineage ST395. *mBio* **5**, e00869 (2014).
34. A. H. Azam, Y. Tanji, Peculiarities of *Staphylococcus aureus* phages and their possible application in phage therapy. *Appl. Microbiol. Biotechnol.* **103**, 4279–4289 (2019).
35. L. De Sordi, M. Lourenço, L. Debarbieux, "I will survive": A tale of bacteriophage-bacteria coevolution in the gut. *Gut Microbes* **10**, 92–99 (2019).
36. S. R. Ables *et al.*, Human oral viruses are personal, persistent and gender-consistent. *The ISME J.* **8**, 1753–1767 (2014).
37. J. L. Baker, B. Bor, M. Agnello, W. Shi, X. He, Ecology of the oral microbiome: Beyond bacteria. *Trends Microbiol.* **25**, 362–374 (2017).
38. S. Paterson *et al.*, Antagonistic coevolution accelerates molecular evolution. *Nature* **464**, 275–278 (2010).
39. A. Buckling, M. Brockhurst, Bacteria-virus coevolution. *Adv. Exp. Med. Biol.* **751**, 347–370 (2012).
40. N. Banahene, H. W. Kavunja, B. M. Swarts, Chemical reporters for bacterial glycans: Development and applications. *Chem. Rev.* **122**, 3336–3413 (2022).
41. J. Mahony, C. Cambillau, D. van Sinderen, Host recognition by lactic acid bacterial phages. *FEMS Microbiol. Rev.* **41**, S16–S26 (2017).
42. F. C. Neuhaus, J. Baddiley, A continuum of anionic charge: Structures and functions of D-alanyl-teichoic acids in gram-positive bacteria. *Microbiol. Mol. Biol. Rev. MMBR* **67**, 686–723 (2003).
43. M. Dunne, M. Hupfeld, J. Klumpp, M. J. Loessner, Molecular basis of bacterial host interactions by gram-positive targeting bacteriophages. *Viruses* **10**, 397 (2018).
44. I. Cota *et al.*, Epigenetic control of *Salmonella enterica* O-antigen chain length: A tradeoff between virulence and bacteriophage resistance. *PLoS Genet.* **11**, e1005667 (2015).
45. M. W. van der Woude, Phase variation: How to create and coordinate population diversity. *Curr. Opin. Microbiol.* **14**, 205–211 (2011).
46. R. Moxon, C. Bayliss, D. Hood, Bacterial contingency loci: The role of simple sequence DNA repeats in bacterial adaptation. *Annu. Rev. Genet.* **40**, 307–333 (2006).
47. N. T. Porter *et al.*, Phase-variable capsular polysaccharides and lipoproteins modify bacteriophage susceptibility in *Bacteroides thetaiotaomicron*. *Nat. Microbiol.* **5**, 1170–1181 (2020).
48. M. C. H. Sørensen *et al.*, Campylobacter phages use hypermutable polyG tracts to create phenotypic diversity and evade bacterial resistance. *Cell Rep.* **35**, 109214 (2021).
49. J. M. Abraham, C. S. Freitag, J. R. Clements, B. I. Eisenstein, An invertible element of DNA controls phase variation of type 1 fimbriae of *Escherichia coli*. *Proc. Natl. Acad. Sci. U.S.A.* **82**, 5724–5727 (1985).
50. M. A. Sánchez-Romero, J. Casadesús, The bacterial epigenome. *Nat. Rev. Microbiol.* **18**, 7–20 (2020).
51. G. L. Murphy, T. D. Connell, D. S. Barratt, M. Koomey, J. G. Cannon, Phase variation of gonococcal protein II: Regulation of gene expression by slipped-strand mispairing of a repetitive DNA sequence. *Cell* **56**, 539–547 (1989).
52. B. Bor *et al.*, Phenotypic and physiological characterization of the epibiotic interaction between TM7x and its basibiont actinomycetes. *Microbial. Ecol.* **71**, 243–255 (2016).
53. J. Tian *et al.*, Acquisition of the arginine deiminase system benefits epiparasitic Saccharibacteria and their host bacteria in a mammalian niche environment. *Proc. Natl. Acad. Sci. U.S.A.* **119**, e2114909119 (2022).
54. J. K. Bedree *et al.*, Quorum sensing modulates the epibiotic-parasitic relationship between actinomycetes odontolyticus and its saccharibacteria epibiont, a nanosynbacter lyticus strain, TM7x. *Front. Microbiol.* **9**, 2049 (2018).
55. R. M. Fisher, L. M. Henry, C. K. Cornwallis, E. T. Kiers, S. A. West, The evolution of host-symbiont dependence. *Nat. Commun.* **8**, 15973 (2017).
56. D. Lindell *et al.*, Transfer of photosynthesis genes to and from *Prochlorococcus* viruses. *Proc. Natl. Acad. Sci. U.S.A.* **101**, 11013–11018 (2004).
57. L. Yang *et al.*, Temperature-dependent carrier state mediated by H-NS promotes the long-term coexistence of *Y. pestis* and a phage in soil. *PLoS Pathog.* **19**, e1011470 (2023).
58. D. N. Mastronarde, Automated electron microscope tomography using robust prediction of specimen movements. *J. Struct. Biol.* **152**, 36–51 (2005).
59. S. Q. Zheng *et al.*, MotionCor2: Anisotropic correction of beam-induced motion for improved cryo-electron microscopy. *Nat. Methods* **14**, 331–332 (2017).
60. J. R. Kremer, D. N. Mastronarde, J. R. McIntosh, Computer visualization of three-dimensional image data using IMOD. *J. Struct. Biol.* **116**, 71–76 (1996).
61. P. Gomez, A. Buckling, Bacteria-phage antagonistic coevolution in soil. *Science* **332**, 106–109 (2011).
62. Q. Zhong *et al.*, Episymbiotic Saccharibacteria TM7x modulates susceptibility of its host bacteria to phage infection and promotes their coexistence. GenBank. <https://www.ncbi.nlm.nih.gov/bioproject?term=PRJNA1037312>. Deposited 9 November 2023.